UNIVERSITY OF CALIFORNIA SAN DIEGO

Anatomy of Cortical Amygdala Circuits that Support Innate Olfactory Valence

A Thesis submitted in partial satisfaction of the requirements
for the degree Master of Science

in

Biology

by

Marlon Blanquart

Committee in charge:

Professor Cory M. Root, Chair
Professor Jing Wang, Co-Chair
Professor Nicholas Spitzer

2022

The Thesis of Marlon Blanquart is approved, and it is acceptable in quality and form for publication on microfilm and electronically.

University of California San Diego

2022

DEDICATION

I would like to dedicate my thesis work to my parents, Veronique and Laurent, for giving their unconditional love and support throughout my entire as a masters student. They were always a phone call away for me day and night. I would also like to dedicate this work to my girlfriend, Liz, for always being a constant source of encouragement and love during the most challenging moments of this program. I would also like to dedicate this work to my friends, Ramon and Sunny, who were always willing to drive me to lab and pick me up from lab at crazy hours. I would also like to dedicate this work to my undergraduate student, Drake, who was always willing to work and learn from me. Lastly, I would like to dedicate this work to my lab mentors, Cory and Donghyung (KDan), for setting a positive environment in the lab, and giving me strength when I had none.

EPIGRAPH

The world ain't all sunshine and rainbows.
It's a very mean and nasty place
And I don't care how tough you are
It will beat you to your knees and keep you
There permanently if you let it.
You, me, or nobody is gonna hit as hard as life.
But it ain't about how hard ya hit,
It's about how hard you can get hit and
Keep moving forward
How much you can take
And keep moving forward.
That's how winning is done!

Rocky Balboa

TABLE OF CONTENTS

THESIS APPROVAL PAGE.....iii

DEDICATION.....iv

EPIGRAPH.....v

TABLE OF CONTENTS.....vi

LIST OF FIGURES.....vii

LIST OF ABBREVIATIONS.....viii

ACKNOWLEDGMENTS.....x

ABSTRACT OF THE THESIS.....xi

INTRODUCTION.....1

MATERIALS/METHODS.....7

RESULTS.....12

DISCUSSION.....18

FIGURES.....22

REFERENCES.....34

LIST OF FIGURES

Figure 1 | Anterograde Tracing of the plCoA Reveals Major Outputs to the NAc, BNST, and MeA.....22

Figure 2 | Retrograde Tracing of the MeA and NAc Reveals plCoA is Topographically Organized Along the Anterior-Posterior (AP) Axis.....23

Figure 3 | Anterograde Tracing of the a-plCoA and p-plCoA Confirms Differential Projections Along the AP axis of the plCoA.....25

Figure 4 | Identification of Collaterals of plCoA Projection Neurons.....27

Figure 5 | Linking Molecularly Distinct Populations in the plCoA with its Topographical AP Axis Using snRNA-seq and *in situ* hybridization.....29

Figure 6 | Anterograde Tracing of *Vglut1* and *Vglut2* Neuronal Populations Reveal Distinct Projection Patterns.....30

Figure 7 | Retrograde Labeling of a-plCoA and p-plCoA Show Both Structures Receive Input Primarily from the Medial and Posterior Piriform Cortex (Pir) 32

LIST OF ABBREVIATIONS

plCoA	Posterolateral Cortical Amygdala
AP	Anterior-Posterior
ML	Medial-Lateral
DV	Dorsal-Ventral
p-plCoA	Posterior Posterolateral Cortical Amygdala
a-plCoA	Anterior Posterolateral Cortical Amygdala
a/p-plCoA	Anterior/Posterior Posterolateral Cortical Amygdala
m-plCoA	Medial Posterolateral Cortical Amygdala
NAc	Nucleus Accumbens
MeA	Medial Amygdala
MOB	Main Olfactory Bulb
BNST	Stria Terminalis
OT	Olfactory Tubercle
PMCo	Posteromedial Cortical Amygdala
AHi	Amygdalohippocampal Area
BMA	Basomedial Amygdala
Pir	Piriform Cortex
BLA	Basolateral Amygdala
a-BLA	Anterior Nucleus of the Basolateral Amygdala
p-BLA	Posterior Nucleus of the Basolateral Amygdala
CeA	Central Amygdala

CxA	Cortex-Amygdala Transition Zone
VP	Ventral Pallidum
ACo	Anterior Cortical Amygdala
EA	Extended Amygdala
AA	Anterior Amygdaloid Area
LOT	Lateral Olfactory Tract
IPAC	Interstitial Nucleus of the Posterior Limb of the Anterior Commissure
IL	Infralimbic Cortex
AIV	Ventral Part of the Agranular Insular Cortex
scRNA-seq	Single Cell RNA Sequencing
snRNA-seq	Single Nucleus RNA Sequencing
ISH	*In situ* hybridization
AAV	Adeno-Associated Virus
Vglut1	Vesicular Glutamate Transporter 1
Vglut2	Vesicular Glutamate Transporter 2
OR	Olfactory Receptors
2PE	2-Phenylethanol
TMT	2,3,5-Trimethyl-3-thiazoline
CTCF	Corrected Total Cell Fluorescence
ID	Integrated Density
AOSC	Area of Selected Cell
MFOBR	Mean Fluorescence of Background Readings

ACKNOWLEDGEMENTS

I would like to acknowledge Professor Cory M. Root for his support as the chair of my committee. His insight and guidance has proved to be invaluable to creating this story.

I would also like to acknowledge Donghyung Lee and James Howe VI for their help with laboratory techniques and data analysis. Their support has helped me in an immeasurable way.

I would also like to acknowledge Drake Jimenez for his commitment to helping me with various laboratory tasks to expedite data acquisition.

The results and figures section, in full, is currently being prepared for submission for publication of the material. The results and figures section is coauthored by Blanquart, Marlon, Howe VI, James, and Chan, Chung Lung. The thesis author was the primary author of this material.

ABSTRACT OF THE THESIS

Anatomy of Cortical Amygdala Circuits that Support Innate Olfactory Valence

by

Marlon Blanquart

Master of Science in Biology

University of California San Diego, 2022

Professor Cory M. Root, Chair
Professor Jing Wang, Co-Chair

The posterolateral cortical amygdala (plCoA) is known to be involved in innate, odor-driven behavioral responses. There are 2 currently debated models in which the plCoA is involved with these behaviors. In one model, the plCoA encodes valence with hardwired circuits capable of driving innate aversive behaviors and the another for innate attractive behaviors, reminiscent of labeled line coding; an opposing model suggests the plCoA uses a population code, whereby valence emerges in downstream areas. Little is known about the connectivity of plCoA, and deciphering the anatomy should help to distinguish between these circuit motifs. To accomplish this, we used anterograde and retrograde tracing experiments to show that the plCoA is

topographically organized on an anterior-posterior (AP) axis based on its outputs, and contains molecularly distinct neuronal populations (*Vglut1* and *Vglut2*) that are also spatially segregated on an anterior-posterior axis. This bifurcating circuitry ultimately reveals the *Vglut1* neurons in the posterior plCoA (p-plCoA) project primarily to the nucleus accumbens (NAc), and the *Vglut2* neurons in the anterior plCoA (a-plCoA) projects primarily to the medial amygdala (MeA). These data reveal a neuronal substrate for valence encoding that is consistent with the plCoA operating with molecularly determined circuitry, ultimately most similar to a labeled line system.

INTRODUCTION

Innate behaviors are defined as actions in response to sensory stimuli, that do not require previous learning and can be found in naïve animals. Innate behaviors can be driven by different sensory systems, but a large number of studies have linked the main olfactory system to essential innate behaviors, such as predator avoidance, or feeding and mating. Mammals perceive smell through a series of events. The odorant molecule travels first through the olfactory epithelium of the nose. Depending on the mammal, the olfactory epithelium contains a large number of odorant (olfactory) receptors (ORs) (Axel, Buck 1991). These ORs are expressed in olfactory sensory neurons, which project to the main olfactory bulb (MOB). Upon reaching the MOB, these olfactory sensory neurons synapse onto the mitral and tufted neurons that project to cortical and subcortical structures (Kandel *et al* 2000).

Mice are an excellent organism to study innate behaviors because odor elicits robust responses, that can be simplified into a single axis of valence (attraction and aversion) with behavioral assays (Root *et al* 2014). Odors can elicit a large number of varying innate behaviors, including feeding/mating (representing positive valence with approach) and freezing/escaping (symbolizing negative valence with avoidance) (Root *et al* 2014; Stowers, Logan 2010). For example, 2-phenylethanol (2PE), a rose oil aroma, was shown to serve as an attractive odorant to mice, whereas 2,3,5-trimethyl-3-thiazoline (TMT), a component of fox secretions, was shown to serve as an aversive odorant to mice (Kobayakawa *et al* 2007; Root *et al* 2014). With these opposing innate behaviors in mind, the neural circuits responsible for contrasting valence remain unknown.

To explain why these opposing innate behaviors occur from different odorants, the neural circuitry between the MOB to subcortical brain structures must be explored. The MOB is known

to project to the posterolateral cortical amygdala (plCoA) (Kevetter, Winans 1981), where different odors elicit different innate behavioral responses. The amygdala is a central processing center structure that regulates emotional behavioral responses (Kevetter, Winans 1981). More specifically, the posterolateral cortical amygdala (plCoA) is a specific nucleus of the amygdala that is commonly referred to as the olfactory amygdala (Ubeda-Bañon *et al* 2007). Another study showed evidence that the mitral-tufted cells of MOB connected to the plCoA are required for innate responses (Root *et al* 2014). Thus, the plCoA plays a significant role in smell perception, and elicits opposing innate behaviors to different odors.

A number of studies suggest there may be some topographic organization in the connection from the MOB to other brain areas. The plCoA receives preferential input form the dorsal MOB (Ghosh 2011), which has been implicated in innate responses to odor (Kobayakawa *et al* 2007). This suggests that the MOB contains a topographic organization. Topographic maps are a common feature of brain organization, whereby different sensory features are mapped to discreet regions. (Patel 2014). Topographic maps can be defined by specific positions within cortical and subcortical brain structures contain different neuroanatomical circuitry, which give rise to different behaviors (Patel 2014).

Topographic organization can be found in many different contexts, where subcortical brain structures can be organized along anatomical axes. Different amygdala studies have shown these structures contain a hard-wired topographic map of valence. For example, a recent study showed the basolateral amygdala (BLA) was spatially segregated on an anterior-posterior axis, of which the anterior nucleus of the BLA (aBLA) projected to the capsular nucleus of the central amygdala and the posterior nucleus of the BLA (pBLA) projected to the lateral and medial nuclei of the central amygdala (Kim *et al* 2016). It was also found that the aBLA neurons were capable of

eliciting place avoidance behaviors, whereas the pBLA neurons were found to elicit place preference behaviors (Kim *et al* 2016). These data indicate that specific amygdala structures contain an anatomical topography. Furthermore, it shows that brain structures can contain anatomically distinct neuronal populations, of which account for opposing behaviors. Another set of results regarding anatomical topography in the BLA was found to project to the central amygdala (CeA) and nucleus accumbens (NAc). In addition, the BLA-CeA projections came primarily from the dorsal BLA, and the BLA-NAc projections came from the medial BLA. The topography from the BLA was also consistent with differences in behavior, where the BLA-CeA circuit primarily elicited negative valence behaviors (aversion), whereas the BLA-NAc circuit primarily prompted positive valence behaviors (attraction) (Beyeler *et al* 2018). These data indicate that subcortical amygdala structures contain topographical organizations from an anatomical standpoint which explains how specific behaviors get activated.

One complexity to topography defined by projections is that most neurons in the brain project to more than one target. Thus, it would be important investigate potential collateral projections. For example, a recent study investigated collateralization in a subset of neurons from the BLA and found they minimally collateralize to multiple downstream targets. After identifying a subpopulation of BLA neurons projected to the NAc, CeA, and ventral hippocampus (vHPC), a clever experiment, using a combination of retrograde and anterograde tracing, was done to test whether the NAc projecting neuron population also project to the NAc, CeA, vHPC, or all three structures. Each of the three BLA projector neuronal populations collateralized to the three main targets; however, the number of neurons projecting to the intended target structure was always greater than in the collateral target structures (Beyeler *et al* 2016). These data shed light on how investigating collateral projections can contribute to understanding whether specific neuronal

populations of interest from the amygdala output to multiple downstream targets equally or more robustly to one.

Topographical organization in the brain is also accompanied by an organization of molecular-determined cell types. One study showed different BLA neuronal populations that projected to different CeA nuclei were molecularly distinct in addition to being spatially segregated; moreover, these two molecularly distinct neurons accounted for opposing behaviors between appetitive and defensive behaviors. Specifically, the BLA *Ppp1r1b*$^{+}$ neurons eliciting appetitive behaviors projected to the lateral and medial nuclei of the CeA, whereas the BLA *Rspo*$^{+}$ neurons eliciting defensive behaviors projected to the capsular nucleus of the CeA (Kim *et al* 2017). This suggests that different amygdala structures can also be molecularly subdivided into different neuronal populations with unique connectivity that ultimately drives for opposing behaviors.

One way to identify molecular neuronal populations is through single-cell RNA sequencing (scRNA-seq). scRNA-seq assesses transcriptional similarities and differences within a biological sample containing thousands of cells, ultimately allowing for quantitative analysis and comparison of mRNA molecules. scRNA-seq is ideal for identifying single cells with unique transcriptomic characteristics, particularly in neurons within the brain (Haque *et al* 2017); however, brain tissues are difficult to dissociate into single cells because neurons contain axons that travel long distances within the brain. That said, a better way to sequence neurons is through single-nucleus RNA-seq (snRNA-seq), as it identifies diagnostic mRNA marker combinations within the nucleus, which can reflect anatomical distinctions between neuron types within brain structures (Alkaslasi *et al* 2021). As such, snRNA-seq is a powerful tool for identifying unique neuronal populations with molecular differences within the same subcortical structure.

Another way to identify specific molecular neuronal populations is through *in situ* hybridization (ISH), which uses DNA/RNA complementary probes labeled with a fluorophore to bind to specific target sequences of neuronal populations. Fluorescence microscopy is then used to visualize the locations of these neurons in the subcortical structure of interest. These probes are used to discover differing neuronal populations (Jensen 2014), which can reveal topographic distributions in certain brain structures.

Recent studies have shown the plCoA is a necessary subcortical structure in eliciting innate, odor-driven behaviors on a positive/negative axis of valence. More specifically, the plCoA was necessary and sufficient for innate behaviors that could either be attractive or aversive to specific odors, and it has been suggested that there may be an axis for valence (Root *et al* 2014). Although the connection between the dorsal MOB and plCoA elicits opposing innate behaviors, it remains unclear if there is spatial organization to the plCoA circuitry. For instance, do different parts of the plCoA have distinct connections to downstream brain areas? If so, are there distinct molecular markers for unique plCoA neurons? If true, this would support the notion of a functional map of innate olfactory valence.

To answer these questions, we wanted to address the anatomical organization of the plCoA by using a combination of anterograde and retrograde tracing. Our goals are to (1) use anterograde AAV tracers to identify all the projections of the plCoA, (2) use retrobead retrograde tracers to determine if the plCoA contains a topographic segregation by looking at cell density populations in the entire plCoA from the medial amygdala (MeA) and NAc, and (3) investigate if the plCoA contains a topographic map by injecting anterograde AAV tracers in spatially segregated portions of the plCoA. Our results indicate the anterior plCoA (a-plCoA) primarily projects to the MeA, whereas the posterior plCoA (p-plCoA) primarily projects to the NAc. Another important question

will be: Do the anterior and posterior plCoA neurons projecting to the NAc or MeA have collaterals to other structures, or is there a one-to-one mapping?

Our results reveal that this bifurcating circuitry exists, where although there is some collateralization between the MeA and NAc from the a-plCoA/p-plCoA, the a-plCoA has a greater number of neurons projecting to the MeA than the NAc and the p-plCoA has a greater number of neurons projecting to the NAc than the MeA. Lastly, we asked whether the plCoA contains molecularly distinct neuronal populations, and if so, do these neuronal populations overlap with the neuronal populations from the spatial segregation of the plCoA? Our results suggest that the plCoA can be divided into at least two molecularly distinct neuronal populations (*Vglut1*$^+$ (*Slc17a7*) and *Vglut2*$^+$ (*Slc17a6*) neurons), where *Vglut1*$^+$ neurons primarily project to the NAc and *Vglut2*$^+$ neurons primarily project to the MeA. This ultimately reveals the plCoA contains a bifurcating circuitry, where the a-plCoA-MeA *Vglut2*$^+$ neurons could play a role in innate aversive behaviors, whereas the p-plCoA-NAc *Vglut1*$^+$ neurons could play a role innate attractive behaviors. This is important for understanding how mammals behave when given odors with innate valence; it might also prove important for humans because it could explain why human brains have a cortical amygdala, and, although still controversial, why humans appear to have innate odor preferences (Arshamian *et al* 2022).

MATERIALS/METHODS

Animals

The animals used for the anterograde a/p-plCoA, retrograde NAc/MeA, collateral tracing, and retrograde a/p-plCoA experiments were C57BL/6 mice purchased from the Jackson Laboratory. *Vglut1*-Cre and *Vglut2*-Cre mice were used for the anterograde *Vglut* experiments. *Vglut1*-Cre and *Vglut2*-Cre mice were bred in house by crossing a $Vglut2^{+}$ or $Vglut1^{+}$ mouse with a C57BL/6 mouse. All of the mice were male and 8 – 12 weeks old at the start of the experiment. These mice were maintained with a reverse 12-hour light/dark cycle with *ad libitum* food and water both before and after surgery.

Stereotaxic Surgery

All surgeries were performed under aseptic conditions using a digital small animal stereotaxic instrument (Kopf Instruments, Tujunga, CA). Mice were first anesthetized in a sealed box containing 5% gaseous isoflurane and were kept under anesthesia (2.5%, 1 L/min) in the stereotaxic system (VetFlo Kent Scientific Corporation, Torrington, CT). 0.04 mL of Ethiqa-XR was used as an analgesic drug to relieve post-operative pain. Optixcare Eye Lube Plus was placed on the mouse's eyes to protect the eyes from dehydration. The skin on the head was removed, then cleaned using betadine and 70% ethanol 3 times. An incision was made to expose the skull. Upon leveling the brain, 1-2 craniotomies were made above the target using a microdrill on the right side of the skull. The anterograde a/p-plCoA experiment had 1 injection in the a-plCoA and another in the p-plCoA. Relative to bregma, the a-plCoA's coordinates were -1.000 anterior-posterior (AP), +2.850 medial-lateral (ML), -6.100 dorsal-ventral (DV), and the p-plCoA's coordinates were -1.600 AP, +3.000 ML, -6.100 DV. The retrograde NAc/MeA experiment had 1 injection in either the NAc or MeA. Relative to bregma, the NAc's coordinates were +1.700 AP, +1.600 ML, -4.600

DV, and the MeA's coordinates were -0.600 AP, +2.100 ML, -5.900 DV. The collateral tracing experiment had 1 injection in the plCoA and the other in either the NAc or MeA. Relative to bregma, the plCoA's coordinates were -1.300 AP, +2.925 ML, -6.100 DV and the NAc/MeA coordinates were the same as previously listed. The *Vglut1/2* experiment had 1 injection in the plCoA. The coordinates for the plCoA were the same as listed before. The retrograde a/p-plCoA experiment had 1 injection in the a-plCoA and the other in the p-plCoA. The coordinates for the a/p-plCoA were the same as listed before. Upon drilling, the pipette capillary glass tip (Drummond) was lowered to the appropriate coordinate over a 5 minute period. 20 nL of virus/retrobeads were injected into the desired structure (50 nL was injected in the MeA, and 300 nL was injected in the NAc) at a rate of 1 nL/second with the Nanoject III device (Drummond). A 15 minute incubation stage was initiated once all volume was dispensed. The pipette capillary glass tip was brought up over a 5 minute period after the 15 minute incubation stage. The mouse's skin was then reattached using Vet bond Glue to cover the skull.

During the entire surgery, the mouse's body temperature was maintained at 36°C with a heating pad. Additionally, the mouse's heart rate, oxygen level, body temperature, and toe pinch response were recorded every 15 minutes. The mouse's body weight was also recorded before the procedure.

Viruses and Retrobeads

The viruses used for the anterograde experiment for the a/p-plCoA surgeries were AAV8-hSyn-ChR2-(H134R)-mCherry (Titer: 2.1×10^{13}) and AAV8-hSyn-ChR2-(H134R)-eYFP (Titer: 3.2×10^{13}) (Salk GT3 Viral Vector Core, La Jolla, CA). Both viruses were used in 1 animal during each surgery, where the viruses were switched off between the a-plCoA and p-plCoA to counterbalance fluorophore expression between the 2 targets, and ultimately control for

differences in expression. The retrobeads used for the retrograde experiment in either the NAc or MeA surgeries were Red Retrobeads (Lumafluor Incorporated, Naples, FL). The viruses used for the collateral tracing experiment were AAVretro-Ef1a-mCherry-IRES-Cre (Titer: 1.7×10^{13}) (Addgene, Watertown, MA), which was injected in either the NAc or MeA, and AAVDJ-Ef1a-DIO-ChR2(H134R)-eYFP-WPRE-pA (Titer: 4.03×10^{13}) (Salk GT3 Viral Vector Core, La Jolla, CA), which was injected in the plCoA. The virus used for the anterograde experiment for the *Vglut1/2* surgeries was AAVDJ-Ef1a-DIO-ChR2(H134R)-eYFP-WPRE-pA, which was injected in the plCoA. The retrobeads used for the retrograde a/p-plCoA experiment were Red IX Retrobeads and Green IX Retrobeads (Lumafluor Incorporated, Naples, FL). Both retrobeads were used in 1 animal during each surgery, where the retrobeads were switched off between the a-plCoA and p-plCoA to counterbalance for labeling efficiency between the 2 targets.

Post-Operative Care

After surgery, the animals were individually housed. Animals were examined daily for their health and well-being. Animals weights were also monitored and recorded every day for a week (7 days) after the surgery. These animals were incubated for 3-5 weeks until euthanization at the end of the experiments.

Euthanasia and Histology

Animals were euthanized after 3-5 weeks of their initial surgery date. Animals were administered ketamine and xylazine for anesthesia and were subject to transcardial perfusion with 10 mL of 1xPBS, followed by a 4% paraformaldehyde 1xPBS solution. The brain was then extracted from the animal, and placed into a 4% paraformaldehyde 1xPBS solution for at least 36 hours until it was sectioned on the vibratome (Leica VT1000S).

All brains were sectioned coronally on the Leica VT1000S vibratome, except for the retrograde NAc/MeA experiment, where the brains were sectioned in a sagittal plane (embedded in 5% agarose in 1xPBS to achieve whole sagittal brain slices). Sagittal sections were done to visualize the entire plCoA on an anterior-posterior axis during statistical analysis. The sections were cut in 50 µm, and mounted on Superfrost Plus microscope slides (Fisher) with DAPI medium (SouthernBiotech). Images were acquired with an Olympus VS120 slide scanner, where the same exposure settings were used every time. A 10x lens was used to scan the slides with a 50 msec exposure time for the DAPI channel, 500 msec exposure time for the FITC channel (to visualize the eYFP or green retrobeads), and 400 msec exposure time for the TRITC channel (to visualize the mCherry or red retrobeads).

For the anterograde *Vglut1/2* experiment, the sections were treated with antibodies (dilution of 1:1000), where the primary antibodies were anti-GFP in goat (Abcam); the secondary antibodies used were anti-Goat with AlexaFluor 488 (Abcam). The sections that were not treated with the antibodies were used for FIJI quantitative analysis since primary and secondary antibodies amplify the signal in a nonlinear manner. Sections that were treated with the antibodies were used as representative images.

FIJI Quantitative Analysis

Quantitative analysis was performed only on brain tissue that had correct targeting. Correct targeting was evaluated by comparing the injection site found in the scanned histology sections with the corresponding brain structure on the Mouse Brain Atlas (Paxinos & Franklin). For the anterograde plCoA, a/p-plCoA, collateral tracing, and *Vglut1/2* experiments, FIJI was used to measure corrected total cell fluorescence (CTCF). For the plCoA, a/p-plCoA and *Vglut1/2* experiments, the fluorescence levels of the synaptic outputs were measured in the entire brain,

whereas for the collateral tracing experiment, the structures were limited to the MeA, NAc, olfactory tubercle (OT), posteromedial cortical amygdala (PMCo), Stria Terminalis (BNST), and amygdalohippocampal area (AHi). The basomedial amygdala (BMA) fluorescence analysis was not included due to viral contamination for all tracing experiments. The CTCF was calculated as described:

$$CTCF = ID - (AOSC \times MFOBR)$$

where ID stands for integrated density, AOSC stands for area of selected cell, and MFOBR stands for mean fluorescence of background readings (The Open Lab Book). These values were converted to an output percentage by taking the CTCF of one output and dividing it by the sum of all CTCFs. The output percentages for the same structure were added up to achieve the total projection percentage.

For the retrograde MeA/NAc and retrograde a/p-plCoA, FIJI was used to measure the total cell count using the Cell Counter Plugin in FIJI. For the retrograde MeA/NAc, only the cells found in the plCoA were quantified. The sagittal brain slices containing the plCoA were then compared to the Mouse Brain Atlas (Paxinos & Franklin) to count the number of cells found per distance away from bregma along the y = -1.3 to -2.5 mm from bregma in increments of 0.1 mm. For the retrograde a/p-plCoA experiment, the cell counts were done in the entire brain. All quantitative analysis was done in a blinded manner by randomly assigning letters to different scanned histology sections to minimize quantification bias.

Statistical Analysis

All data are shown as mean and SEM. The thresholds for significance were placed at $^{*}p < 0.05$, $^{**}p < 0.01$, $^{***}p < 0.001$, and $^{****}p < 0.0001$ where paired, unpaired student's t-test, and ANOVA test were done on GraphPad Prism.

RESULTS

The plCoA Projects to Structures Involved in Innate Valence and Olfaction

We hypothesized that the plCoA is topographically organized and contains molecularly distinct neurons on an AP axis to account for the differences in behavior between innate attraction and aversion. If this hypothesis is true, it can be predicted that the plCoA contains a bifurcating circuitry both anatomically and molecularly. To test this, Chung Lung Chan, PhD., first injected a Cre-dependent AAV virus (AAVDJ-hSyn-FLEX-mRuby-T2A-SynEGFP) with a Cre-expressing AAV virus (AAV5-EF1A-Cre) to explore all the outputs of the plCoA (**figure 1a**). I quantified the mean CTCF values of all the projections from the plCoA. Structures that had a mean projection volume greater than the mean plCoA fluorescence were counted (i.e. the projection volume needed to be greater than 1). The main structures found to project from the plCoA included the NAc (3.3 A.U.), BNST (3.0 A.U.), MeA (1.9 A.U.), Piriform Cortex (Pir) (1.5 A.U.), BLA (1.2 A.U.), AHi (1.1 A.U.), and PMCo (1.1 A.U.) with a sample size of n = 5 mice (**figure 1c**). Upon finding and quantifying key projections of the plCoA, the NAc (**figure 1bii**) and MeA (**figure 1biv**) were further explored because of their known roles in reward seeking and defensive behaviors, respectively. This was done to see if the plCoA contained a topographic map of neuron with particular projection targets.

Retrograde Tracing of the plCoA Outputs to the NAc and MeA are Organized on an AP Axis

We hypothesized that one portion of the plCoA projected primarily to the NAc and another portion projected primarily to the MeA. We defined the boundaries of the plCoA as -1.3 to -1.7 for the anterior plCoA (a-plCoA), -1.8 to -1.9 for the medial plCoA (m-plCoA), and -2.0 to -2.5 for posterior plCoA (p-plCoA) (all coordinates are distances relative to bregma in millimeters, according to Paxinos & Franklin). To do this, 300nL of red retrobeads were injected in the NAc

unilaterally, which resulted in the majority of the NAc inputs being found in the p-plCoA; moreover, 50nL of red retrobeads were injected in the MeA unilaterally, which resulted in the majority of the MeA inputs being found in the a-plCoA (**figure 2a**). The associated images show a clear bias of inputs for the p-plCoA from the NAc and clear bias of inputs for the a-plCoA from the MeA (**figure 2b**). More specifically, within the p-plCoA, 83.2±0.7% of outputs were to the NAc and 16.8±0.4% were to the MeA. On top of that, within the a-plCoA, 30.5±0.2% of outputs were to the NAc and 69.5±1.3% were to the MeA. However, within the m-plCoA, there were no statistically significant differences between outputs to the NAc (53.4±0.4%) and MeA (46.6±0.7%) (**figure 2c**). This was done over n = 8 mice (4 NAc mice and 4 MeA mice). From there, we wanted to take a closer look at the percentage of projection neurons throughout the entire plCoA by plotting the percentage of neurons projecting to the NAc or MeA at each distance from bregma (spanning from -1.3 to -2.5 mm from bregma). The data revealed the majority of the projections to the NAc were from the p-plCoA and the majority of projections to the MeA were from the a-plCoA (**figure 2d**).

Anterograde Tracing of a/p-plCoA Outputs Suggest Topographic Organization on AP Axis

To further confirm this topographic mapping of the plCoA on an AP axis, anterograde tracing using 2 AAVs with either a red or green reporter in either the a-plCoA or p-plCoA was done within one animal (**figure 3a**). The viruses were switched off between the a-plCoA and p-plCoA to counterbalance fluorophore expression between the 2 targets to permit more accurate quantification. We hypothesized that because the retrograde data showed a clear separation of the plCoA neurons projecting to the NAc and MeA (a-plCoA primarily projects to MeA and p-plCoA primarily projects to NAc), this a/p-plCoA anterograde experiment should show the same result. As can be seen in the representative images, the a-plCoA projects primarily to the MeA and the p-

plCoA projects primarily to the NAc (**figure 3b**). The normalized percentage outputs revealed the a-plCoA (n = 5) projects more to the MeA (7.7±0.9%) than the p-plCoA (4.4±0.5%) (n = 4); moreover, the normalized percentage outputs showed the p-plCoA projects more to the NAc (5.2±1.0%) than the a-plCoA (2.2±0.4%) (**figure 3c**). This anterograde experiment, thus, supports the retrograde data seen before.

The plCoA-NAc and plCoA-MeA Circuits Contain Little Collateral Projections

Thus far, we have found that neurons projecting to the NAc and MeA are distinct and anatomically segregated. However, it remains unclear whether these neurons have collateral projections to other structures. For example, we wanted to determine if the neurons projecting from the plCoA to the NAc also project to the BNST or other regions. We hypothesized that there would be little to no collaterals to the MeA in the plCoA-NAc circuit and little to no collaterals to the NAc in the plCoA-MeA circuit, but there could be collaterals to other structures. To investigate this, we combined retrograde tracing from the NAc and MeA to express cre in the plCoA, with anterograde tracing from the plCoA using a cre-dependent reporter. We injected a retro AAV virus expressing Cre (AAVretro-EF1A-mCherry-IRES-Cre) into either the NAc or MeA and injected a Cre-dependent eYFP AAV virus in the plCoA (AAVDJ-Ef1A-DIO-ChR2(H134R)-eYFP-WPRE-pA) (**figure 4a**). The associated representative images for the plCoA-NAc show a clear output bias back to the NAc with low collateral output percentage to the other outputs; moreover, the plCoA-MeA shows a clear output bias back to the MeA with low collateral output percentage to the other outputs (**figure 4b**). The six structures we decided to focus on were the NAc, MeA, BNST, AHi, PMCo, and olfactory tubercle (OT) since those structures receive more input from the plCoA than some other minor targets. Within the plCoA-NAc circuit, the majority of the axons from NAc-projecting neurons were found in the NAc, OT, and BNST (n = 5); within the plCoA-MeA circuit,

the majority of the axons from MeA-projecting neurons were found in the MeA, OT, and PMCo (n = 8) (**figure 4c**). These data reveal the NAc-projecting neurons output minimally to the MeA and the MeA-projecting neurons output minimally to the NAc, further suggesting the neurons projecting to the NAc and MeA are distinct.

Linking Molecularly Distinct Populations in the plCoA with its Topographical AP Axis Using snRNA-seq and *in situ* Hybridization

Up to this point, we found the plCoA contains distinct neuronal populations that project to the MeA and NAc with little collateral downstream projections. However, we wanted to explore the molecular properties of these different neuronal populations to see if they could account for these different projection patterns. To explore this, James Howe VI dissected a section of the a-plCoA and p-plCoA, cryopreserved and pooled the tissue, isolated specific nuclei based on nuclear fluorescence with fluorescence-activated nuclei sorting (FANS), and sequenced the RNA using a cDNA library preparation (**figure 5a**). Upon finding that plCoA neurons display many differences in gene expression, we found 2 molecularly different neuronal populations that were enriched in opposing sides of the plCoA on an AP axis. More specifically, we found the a-plCoA contained significantly greater proportion of *Vglut2*$^{+}$ neurons and the p-plCoA contained significantly more *Vglut1*$^{+}$ neurons (**figure 5b**). The proportion reflecting equal numbers *Vglut1 and Vglut2* in one area was lower than 0.5 (indicated by the dashed line), because more a-plCoA cells were sequenced via snRNA-seq. This topographical distribution of *Vglut1*$^{+}$and *Vglut2*$^{+}$neurons is further supported by *in situ* hybridization from the mouse brain atlas (**figure 5c**) (Allen Institute for Brain Science, 2004, Lein *et al*., 2007).

Anterograde Tracing of *Vglut1* and *Vglut2* Distinct Neuronal Populations Reveals Unique Projection Patterns.

The previous experiment showed the two main markers in the plCoA was *Vglut1* and *Vglut2* are topographically expressed. We next sought to test whether these molecularly distinct neurons found in the plCoA have distinct projection targets, consistent with an overlap between a topographic and molecular organization of the plCoA. A Cre-dependent AAV virus (AAVDJ-Ef1a-DIO-ChR2(H134R)-eYFP-WPRE-pA) was injected into the plCoA of either *Vglut1-Cre* or *Vglut2-Cre* animals (**figure 6a**). Given that *Vglut1* and *Vglut2* are restricted to the posterior and anterior regions, respectively, and these regions have distinct projections, we hypothesized that the *Vglut1-Cre* animals would primarily project to the NAc, and the *Vglut2-Cre* animals would primarily project to the MeA, consistent with the fact that $Vglut1^+$neurons are found primarily in the p-plCoA and $Vglut2^+$neurons are found primarily in the a-plCoA. As can be seen in the representative images, the *Vglut1-Cre* animals show an output bias to the NAc and an output bias to the MeA for the *Vglut2-Cre* animals (**figure 6b**). The normalized percentage outputs revealed $Vglut1^+$ neurons (n = 5) projects more to the NAc (9.9±1.9%) than $Vglut2^+$ neurons (n = 4) (3.5±0.8%); moreover, the normalized percentage outputs revealed $Vglut2^+$ neurons projects more to the MeA (14.4±2.9%) than $Vglut1^+$ neurons (5.7±1.4%) (**figure 6c**). Overall, these data suggest the a/p-plCoA contain molecularly distinct neurons that have distinct outputs.

Retrograde Labeling of a-plCoA and p-plCoA Show Both Structures Receive Input Primarily from the Medial and Posterior Piriform Cortex

Lastly, to capture a more complete picture of all the inputs/outputs for the plCoA, we decided to conduct a retrograde tracing experiment on the a-plCoA and p-plCoA. We hypothesized there could be significant differences in the plCoA's inputs, since they have different outputs,

reflecting different functions. To conduct this experiment, we injected green and red retrobeads into either the a-plCoA or the p-plCoA, where the retrobeads were counterbalanced between the a-plCoA and p-plCoA to permit more accurate quantification and maximize labeling efficiency (**figure 7a**). Due to too little signal to noise ratio, we could not detect bright enough signal in the MOB to successfully quantify it; however, we were able to find that the majority of the other inputs were from the Pir (notably layer 2 of the Pir) (**figure 7b**). The percentage of neurons projecting to either the a/p-plCoA were primarily from the Pir (66.4±2.8% for a-plCoA and 67.5±2.5% for p-plCoA), but other structures like the agranular insular cortex (AIV), anterior cortical amygdala (ACo), cortex-amygdala transition zone (CxA), PMCo, and MeA (**figure 7c**). We then decided to take a closer look at the Pir to see if there was a specific plane of the Pir that projected the most to the a-plCoA and p-plCoA. Because the Pir changes in size along the AP axis, we decided to normalize to the size by taking the number of neurons counted and dividing it by the area of the anterior, medial, and posterior Pir. From there, we calculated the relative percentage of input neurons per area. These data revealed a significant increase in plCoA input from both the medial and posterior Pir relative to the anterior Pir in both the a/p-plCoA (**figure 7d**). As such, on top of receiving input from the dorsal MOB (Ghosh 2011), it would appear the plCoA also receives input from the medial and posterior Pir.

Acknowledgements

The results section, in full, is currently being prepared for submission for publication of the material. The results and figures section is coauthored by Blanquart, Marlon, Howe VI, James, and Chan, Chung Lung. The thesis author was the primary author of this material.

DISCUSSION

The results derived from these tracing experiments ultimately reveal a spatial and molecular organization of the plCoA. The major outputs of the plCoA were found to be the NAc, BNST, BMA, MeA, Pir, BLA, and PMCo. We focused on the NAc and MeA for further exploration, because of their associated role in valence behaviors, and found that the plCoA contains a bifurcating circuitry for the NAc and MeA. Retrograde labeling of the plCoA from either the NAc and MeA suggested that the MeA received the majority of inputs from the a-plCoA and the NAc received the majority of inputs from the p-plCoA. This was further confirmed through anterograde tracing of the plCoA by comparing the outputs of the a-plCoA and p-plCoA, which showed that the a-plCoA projects mainly to the MeA and the p-plCoA projects mainly to the NAc. Given that most neurons have collateral projections, we characterized collaterals of NAc- and MeA-projecting neurons, and found that the plCoA-MeA circuitry showed very little collateral projections to the NAc; the plCoA-NAc circuitry also showed little collateral projections to the MeA, indicating that these represent distinct circuits. It is important to note that other collaterals from both populations were identified, but these were minor in comparison to the NAc- or MeA-specific projections. Collectively, these data indicate that the plCoA is topographically organized on an anterior-posterior axis with circuits that may support behavioral valence.

To determine if there are molecularly distinct neuronal populations between the anterior and posterior plCoA, snRNA-seq and *in situ* hybridization were done. The results ultimately showed the plCoA contained 2 molecularly distinct neuronal populations that could be identified by *Vglut1* and *Vglut2*. Furthermore, they were also spatially segregated, whereby the *Vglut1* population of neurons was primarily found in the p-plCoA and *Vglut2* population of neurons was primarily found in the a-plCoA. The projections of these molecularly distinct neurons was assessed

through anterograde tracing of *Vglut1-Cre* and *Vglut2-Cre* animals, revealing that the *Vglut1-Cre* neurons primarily had projections to the NAc and *Vglut2-Cre* neurons primarily had projections to the MeA. Lastly, the plCoA's inputs were explored, where the medial and posterior Pir were found to be the main higher-order structure that projects to both the a-plCoA and p-plCoA. Although differences in inputs from the MOB might be expected, unfortunately, due to poor fluorescence visualization from the retrobeads in the MOB, the MOB could not be included as part of the quantification process of the inputs of the a/p-plCoA. Thus, we conclude that the a/p-plCoA gets most of its higher order inputs from the medial and posterior Pir; additionally, the plCoA contains a topographic and molecular organization on an AP axis, where the a-plCoA contains primarily *Vglut2* neurons that project mainly to the MeA and the p-plCoA contains primarily *Vglut1* neurons that project mainly to the NAc.

There are 2 currently debated models involving how the plCoA is involved with innate, odor-driven behaviors on a valence axis. One model suggests that there is a neural circuit that connects the MOB and the plCoA, and it is the plCoA that separates innate aversive and appetitive behaviors through distinct connections, reminiscent of labeled lines. This was supported by optogenetically activating different odor-responsive neurons within the plCoA that drove opposite valence behaviors. Photoactivation of the plCoA neurons that responded to TMT (a component of fox urine that mice innately avoid) resulted in increased avoidance and freezing behavior of mice, whereas photoactivation of the plCoA neurons that responded to 2-PE (a rose oil aroma that mice are innately attracted to) resulted in increased attraction behaviors. Further, these odor-labeled neurons were topographically distributed. This would ultimately imply there are odor-responsive neurons within the plCoA that are responsible for mediating these 2 opposing innate, odor-driven behaviors (Root *et al* 2014). An alternative model suggests that the plCoA does not contain a

spatial mapping to account for the differences in innate, odor-driven behaviors; as such, this suggests the plCoA uses a distributed population code to be read out by downstream subcortical structures, which could encode for this valence of odor-driven behaviors. In support of this, multi-shank silicon probes were targeted to the plCoA for electrical recording, where the animal was presented odors (including TMT or 2-PE) for 2 seconds. The neurons along the AP axis of the plCoA did not show a selective response to odor valence. Instead, they found that there could be a population code that could encode odor identity, but not valence. As such, the plCoA is unlikely to contain valence-specific neurons. Instead, the plCoA would rely on a complex population code, where the valence readout is performed downstream (Iurilli 2017).

Our data supports a model that the plCoA is indeed topographically mapped on an AP axis with bifurcating circuitry capable of supporting valence encoding. How can we reconcile our findings with that of Iurilli 2017? First, there are a few technical concerns: The placement of the silicon probes in their recordings appear to largely target the middle and posterior regions and it is unclear how restricted the probes were to the plCoA, opening the possibility they did not record from the same subregions of the plCoA (e.g. a-plCoA). Second, the 2 second odor stimulation, although commonly used, does not reflect the timescale for innate olfactory behaviors (seconds vs minutes). It is possible that longer odor exposure leads to more selectivity that arises through a combination of feedforward excitation and local interactions. In addition to the technical considerations, conceptually, this population code model would not expect that there are neurons with distinct molecular and circuit properties that bifurcate to support valence. It is also noteworthy that they acknowledge the possibility that the identified population code exists embedded within valence encoding neurons that eluded their recordings. Our data indicate there are 2 molecularly distinct neuronal populations throughout the plCoA segregated along the AP axis, with distinct

projections to areas associated with behavioral valence. Thus, our findings support a model in which plCoA neurons with distinct projections would be likely to respond selectively to odors valence. However, their odor tuning remains to be directly investigated.

The plCoA is known to play a role in both innate attractive and aversive behaviors. Our findings establish the cell types and circuitry that may underlie these behaviors of opposing valence. The mitral tufted cells of the MOB (Buck 2004) project to the plCoA to drive innate responses to odor (Root *et al* 2014). We propose that within the plCoA, if the odor is attractive (like 2-PE), this will activate the *Vglut1*$^+$ neurons in the p-plCoA, that project to the NAc, making the mouse attracted to that odor since this odor activates an innate, odor-driven attractive behavior. On the other hand, if the odor is aversive (like TMT), this will activate *Vglut2*$^+$ neurons in the a-plCoA, that project to the MeA, making the mouse repulsed to that odor. In this model, *Vglut1*$^+$ and *Vglut2*$^+$ neurons should receive different inputs from glomeruli in the MOB, whereby distinct glomeruli that mediate attraction and aversion should preferentially target *Vglut1*$^+$ and *Vglut2*$^+$ neurons, respectively. Further, it remains to be determined what function is served by the Pir projection to the plCoA, but it is striking that it is one of the main inputs. Identification of these cell types and circuitry will afford a framework for more targeted neural recordings and manipulation in the future. Lastly, the plCoA is a conserved brain region found in rodents and primates. Ultimately, this neuroanatomical bifurcation may define the anatomical substrate for innate odor-driven behavior in mice, which could offer clarity on this pathway in other mammals, including humans.

FIGURES

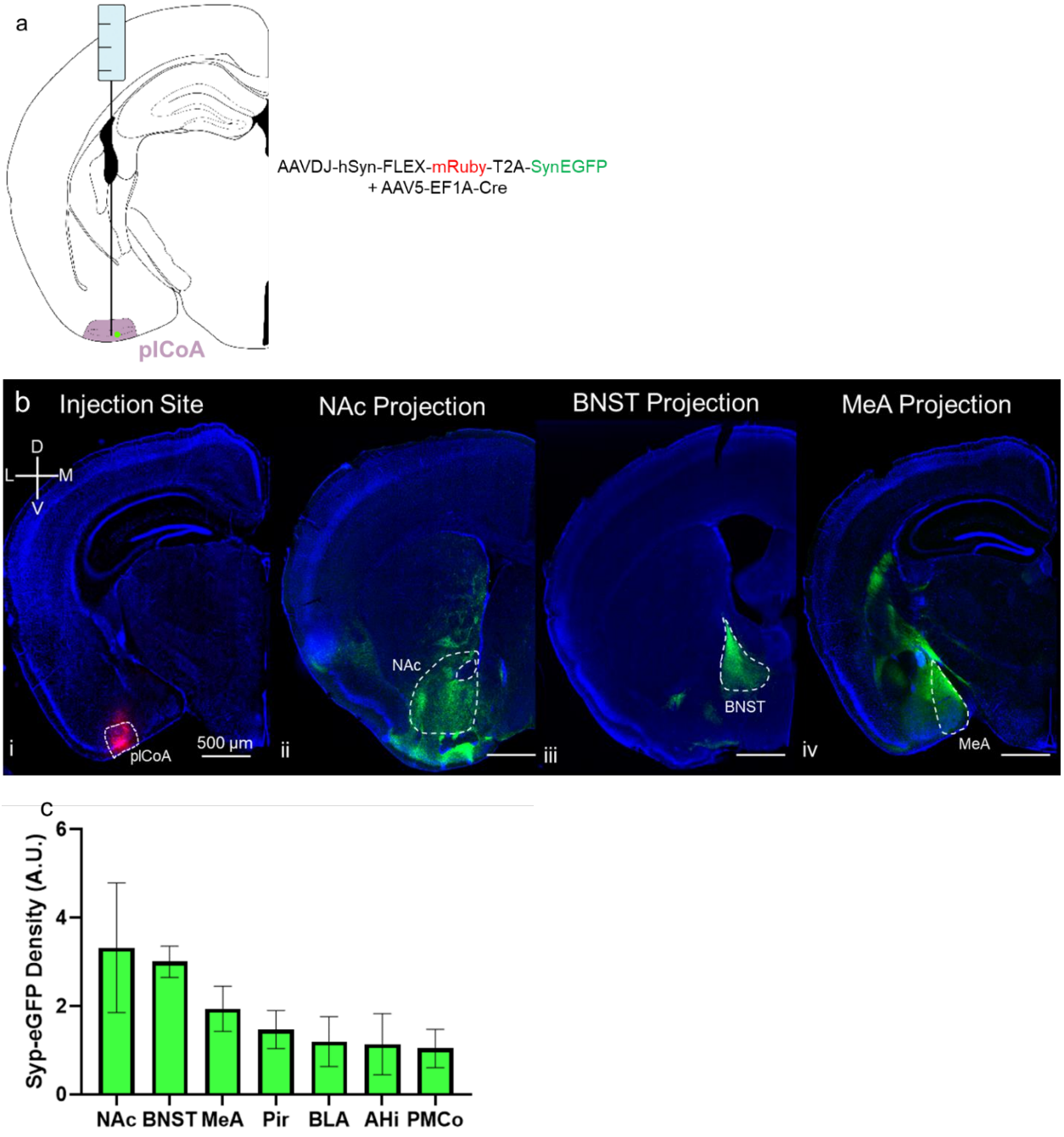

Figure 1 | Anterograde Tracing of the plCoA Reveals Major Outputs to the NAc, BNST, and MeA. Injection of synaptophysin AAV and Cre-expressing AAV viruses show majority expression in the NAc, BNST, and MeA. **a**: Schematic of a coronal section showing injection of AAVDJ-hSyn-FLEX-mRuby-T2A-SynEGFP and AAV5-EF1a-Cre viruses into the plCoA. **b**: Representative images of injection in plCoA to show proper targeting (**i**) and major projections of the plCoA including the NAc (**ii**), BNST (**iii**), and MeA (**iv**). **c**: The synaptic density was quantified relative to the plCoA's fiber density was quantified, where only the outputs that had a relative fiber density greater than 1 were included (n = 5).

Figure 2 | Retrograde Tracing of the MeA and NAc Reveals plCoA is Topographically Organized Along the Anterior-Posterior (AP) Axis. Injection of red retrobeads into either MeA or NAc show the MeA receives input primarily from the anterior plCoA (a-plCoA) and the NAc receives input primarily from the posterior plCoA (p-plCoA). **a**: Schematic of a sagittal section showing injection of red retrobeads into either the MeA or NAc. **b**: Representative images of the MeA inputs in the a-plCoA with red retrobead injection site in the MeA and NAc inputs in the p-plCoA with red retrobead injection of the NAc, anterior is on the left. **c**: The percent of plCoA neurons labeled from either the MeA or NAc (n = 4 for the MeA and n = 4 for the NAc) divided along an AP axis (m-plCoA being the medial plCoA), showing a larger percentage of neurons projecting to the MeA being found in the a-plCoA and a larger percentage of neurons projecting to the NAc being found in the p-plCoA. **p < 0.01, ****p < 0.0001, unpaired t-test comparing MeA and NAc inputs; error bars, s.e.m. **d**: The percent of plCoA neurons labeled projecting to either the MeA or NAc (n = 4 for the MeA and n = 4 for the NAc) as a function of the distance from bregma, showing a larger percentage of neurons projecting to the MeA in the a-plCoA (-1.3 to -1.7 mm) and a larger percentage of neurons projecting to the NAc in the p-plCoA (-2.0 to -2.5 mm). *p < 0.05, unpaired t-test comparing each MeA and NAc percentage input; error bars, s.e.m.

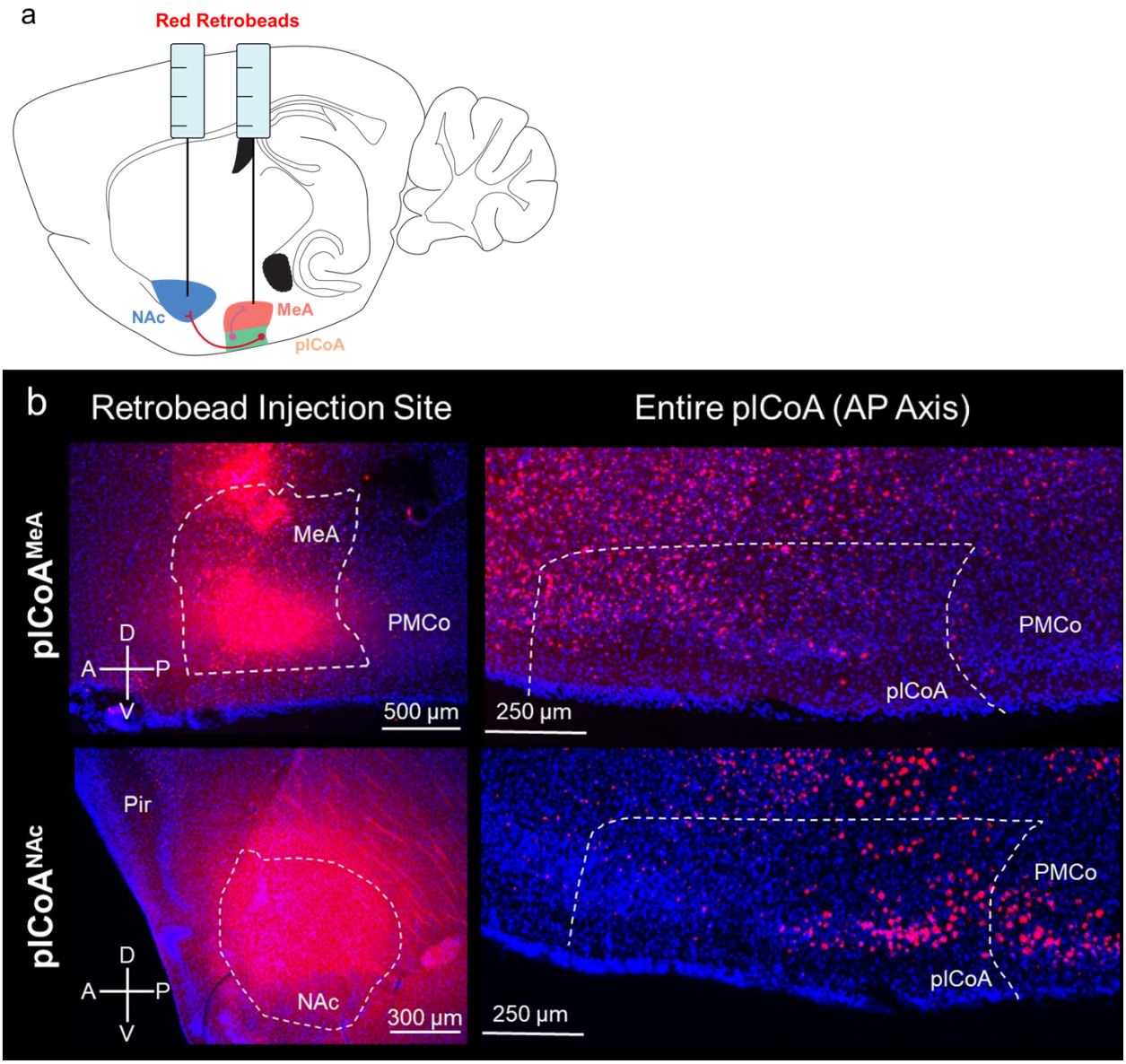
a
Red Retrobeads
NAc
MeA
plCoA
b
Retrobead Injection Site
Entire plCoA (AP Axis)
plCoA MeA
MeA
PMCo
D
A
P
V
500 µm
250 µm
plCoA
plCoA NAc
Pir
NAc
300 µm
c
% plCoA Neurons Labeled
100
80
60
40
20
0
**
n.s.
****
a-plCoA
m-plCoA
p-plCoA
plCoA MeA
plCoA NAc
d
% plCoA Neurons Labeled
30
20
10
0
-1.5
-2.0
-2.5
Distance from Bregma (mm)
plCoA MeA
plCoA NAc

Figure 3 | Anterograde Tracing of the a-plCoA and p-plCoA Confirms Differential Projections Along the AP axis of the plCoA. Injection of AAV viruses with red or green reporters into either the a-plCoA or p-plCoA confirms retrograde tracing from MeA or NAc, suggesting the a-plCoA primarily projects to the MeA and p-plCoA primarily projects to the NAc. **a**: Schematic of a coronal section showing the injection of either AAV8-hSyn-ChR2(H134R)-mCherry or AAV8-hSyn-ChR2(H134R)-eYFP into either the a-plCoA or p-plCoA (viruses were counterbalanced between a/p-plCoA animals). **b**: Representative images of the mCherry virus injected into the a-plCoA and eYFP virus injected in p-plCoA (**i**), the mCherry virus projection patterns in the NAc/MeA (**ii**), the eYFP virus projection patterns in the NAc/MeA (**iii**), and the merged mCherry and eYFP virus projection patterns in the NAc/MeA (**iv**). **c**: All the output percentages from the a-plCoA and p-plCoA, revealing that there are some significant differences between anterior and posterior projection targets, including the NAc and MeA ($n = 5$ for a-plCoA and $n = 4$ for p-plCoA). *$p < 0.05$, **$p < 0.01$, ****$p < 0.0001$ unpaired t-test comparing a-plCoA and p-plCoA outputs; error bars, s.e.m.

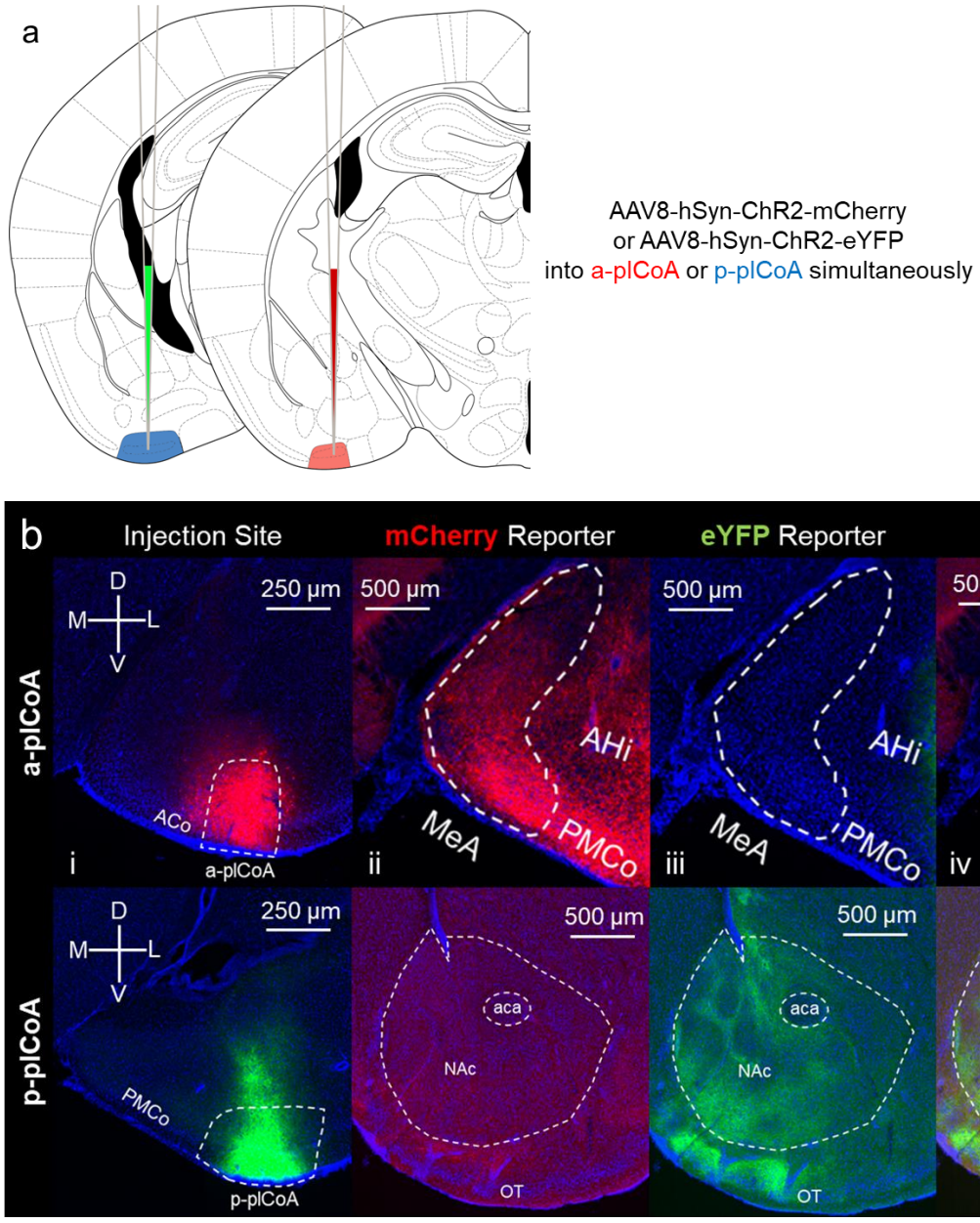
a
AAV8-hSyn-ChR2-mCherry
or AAV8-hSyn-ChR2-eYFP
into a-plCoA or p-plCoA simultaneously
b
Injection Site
mCherry Reporter
eYFP Reporter
Merged
a-plCoA
p-plCoA
D
M
L
V
250 μm
500 μm
ACo
a-plCoA
AHi
MeA
PMCo
i
ii
iii
iv
aca
NAc
OT
C
Output % from plCoA
30
20
10
0
a-plCoA
p-plCoA
PMCo
Pir
CeA
AHi
BNST
NAc
OT
MeA
ACo
EA
AA
AIV
VP
CxA
LOT
IPAC
IL
****
**
*

Figure 4 | Identification of Collaterals of plCoA Projection Neurons. Injection of AAV Cre-dependent and AAVretro Cre-expressing viruses show small amounts of collateral projections to unintended target structures. **a**: Schematic of a coronal section showing the injection of AAVretro-EF1a-mCherry-IRES-Cre either in the NAc or MeA and injection of AAVDJ-EF1a-DIO-ChR2(H134R)-eYFP-WPRE-pA in the plCoA in the same animal. **b**: Representative images of the AAVretro-cre-mCherry virus injected in the NAc or the MeA (**i**), AAVDJ-DIO-ChR2-eYFP injected in the plCoA for either the plCoA-MeA projection pattern or the plCoA-NAc projection pattern (**ii**), and the NAc outputs of plCoA-MeA and plCoA-NAc projection patterns (**iii**) and MeA outputs of plCoA-MeA and plCoA-NAc projection patterns (**iv**). **c**: The output percentages from the plCoA-MeA and plCoA-NAc were to the major projections from figure 1, where the largest neuron projection percentage of the plCoA-MeA projection pattern went back to the MeA and the largest neuron projection percentage of the plCoA-NAc projection pattern went back to the NAc ($n = 8$ for the plCoA-MeA and $n = 5$ for the plCoA-NAc). *$p < 0.05$, **$p < 0.01$, ****$p < 0.0001$, unpaired t-test comparing output percentages between plCoA-MeA and plCoA-NAc; error bars, s.e.m.

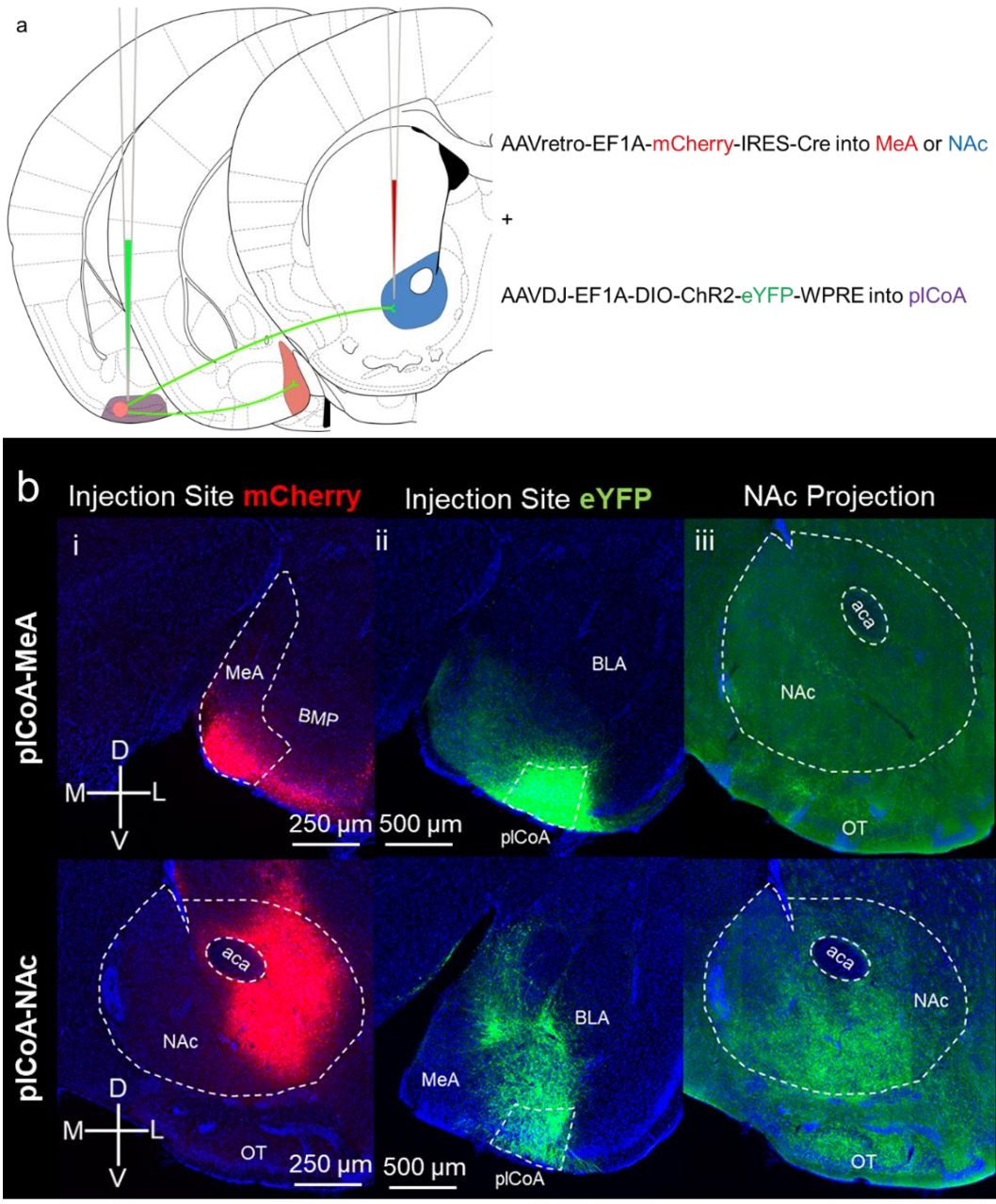
a
AAVretro-EF1A-mCherry-IRES-Cre into MeA or NAc
+
AAVDJ-EF1A-DIO-ChR2-eYFP-WPRE into plCoA
b
Injection Site mCherry
Injection Site eYFP
NAc Projection
MeA Projection
i
ii
iii
iv
plCoA-MeA
MeA
BMP
BLA
aca
NAc
OT
plCoA
D
M
L
V
250 µm
500 µm
plCoA-NAc
C
% Outputs from plCoA
60
40
20
0
plCoA-MeA
plCoA-NAc
****
*
**
AHi
MeA
NAc
OT
PMCo
BNST

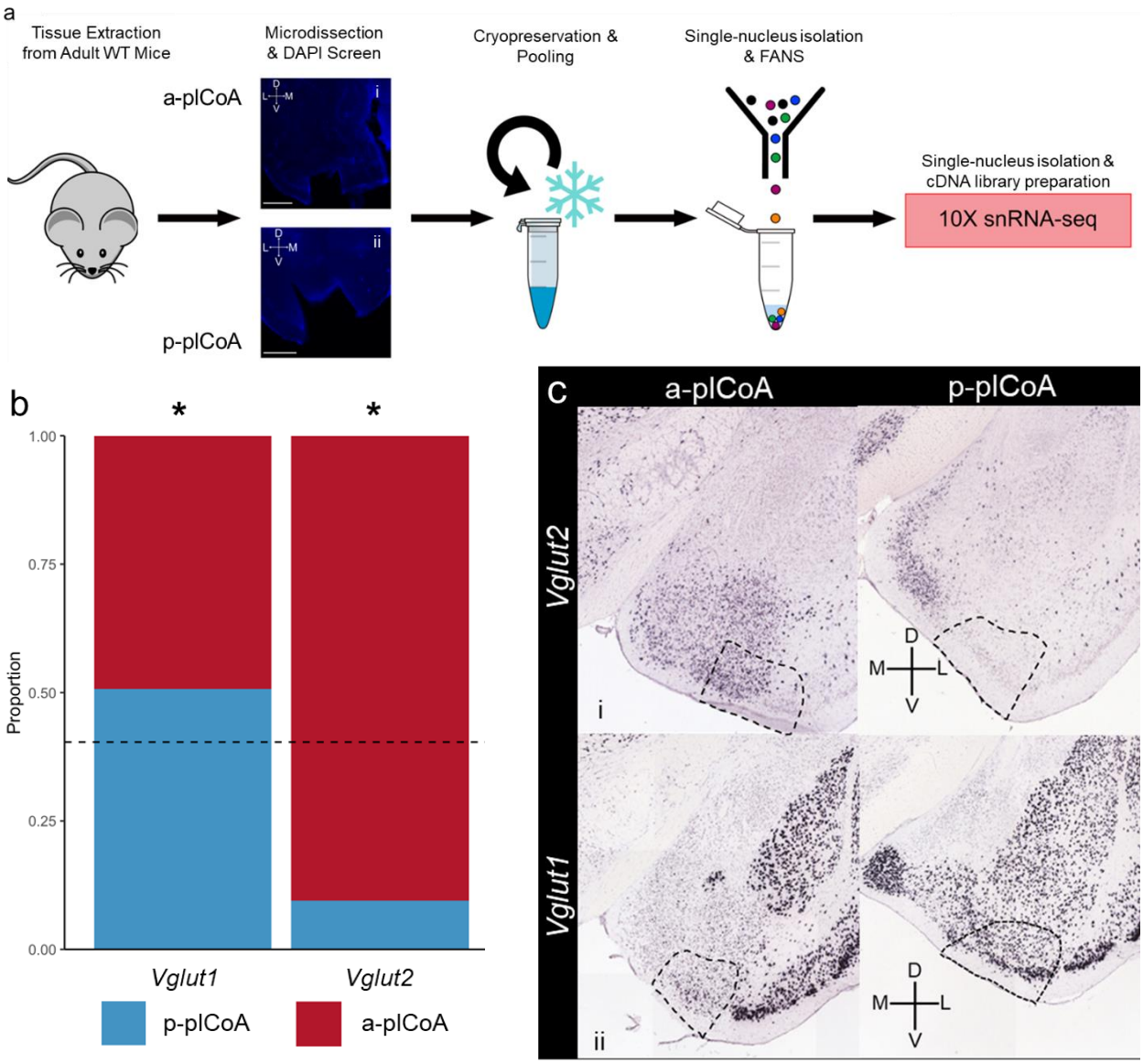

Figure 5 | Linking Molecularly Distinct Populations in the plCoA with its Topographical AP Axis Using snRNA-seq and *in situ* hybridization. Distribution of *Vglut1* and *Vglut2* neuronal populations found in distinct portions of the plCoA on an AP axis. **a**: Schematic of how the snRNA-seq was done on the a-plCoA (**i**) and p-plCoA (**ii**). **b**: The proportion of *Vglut1*$^+$ neurons compared to *Vglut2*$^+$ neurons in the a/p-plCoA, where the majority of *Vglut2*$^+$ neurons are in the a-plCoA and the majority of *Vglut1*$^+$ neurons are in the p-plCoA. **ci**: Representative images showing the majority of *Vglut2*$^+$ neurons are in the a-plCoA. Allen Mouse Brain Atlas, https://mouse.brain-map.org/experiment/show/73818754. **cii:** Representative images showing the majority of *Vglut1*$^+$ neurons are in the p-plCoA. Allen Mouse Brain Atlas, https://mouse.brain-map.org/gene/show/48802. *p < 0.05, ANOVA test comparing *Vglut1* and *Vglut2* neuronal populations within the plCoA.

Figure 6 | Anterograde Tracing of *Vglut1* and *Vglut2* Neuronal Populations Reveal Distinct Projection Patterns. Injection of AAV Cre-dependent eYFP virus showing that the *Vglut1*$^+$ neurons project more to the NAc relative to the MeA and *Vglut2*$^+$ neurons project more to the MeA relative to the NAc. **a**: Schematic of a coronal section showing the injection of AAVDJ-EF1A-DIO-ChR2(H134R)-eYFP-WPRE-pA in the plCoA. **b**: Representative images of the eYFP virus injected into the plCoA (**i**), the eYFP virus projection patterns in the MeA (**ii**), the eYFP virus projection patterns in the NAc (**iii**). All images were stained with eYFP antibodies. **c**: The output percentages from the *Vglut1* and *Vglut2* neuronal populations to all downstream projections, where a larger projection percentage of the *Vglut2*$^+$ neurons to the MeA relative to the NAc and a larger neuron projection percentage of the *Vglut1*$^+$ neurons to the NAc relative to the MeA (n = 5 for *Vglut2* and n = 4 for *Vglut1*). *$p < 0.05$, **$p < 0.01$, unpaired t-test comparing *Vglut1* and *Vglut2* neuronal outputs; error bars, s.e.m.

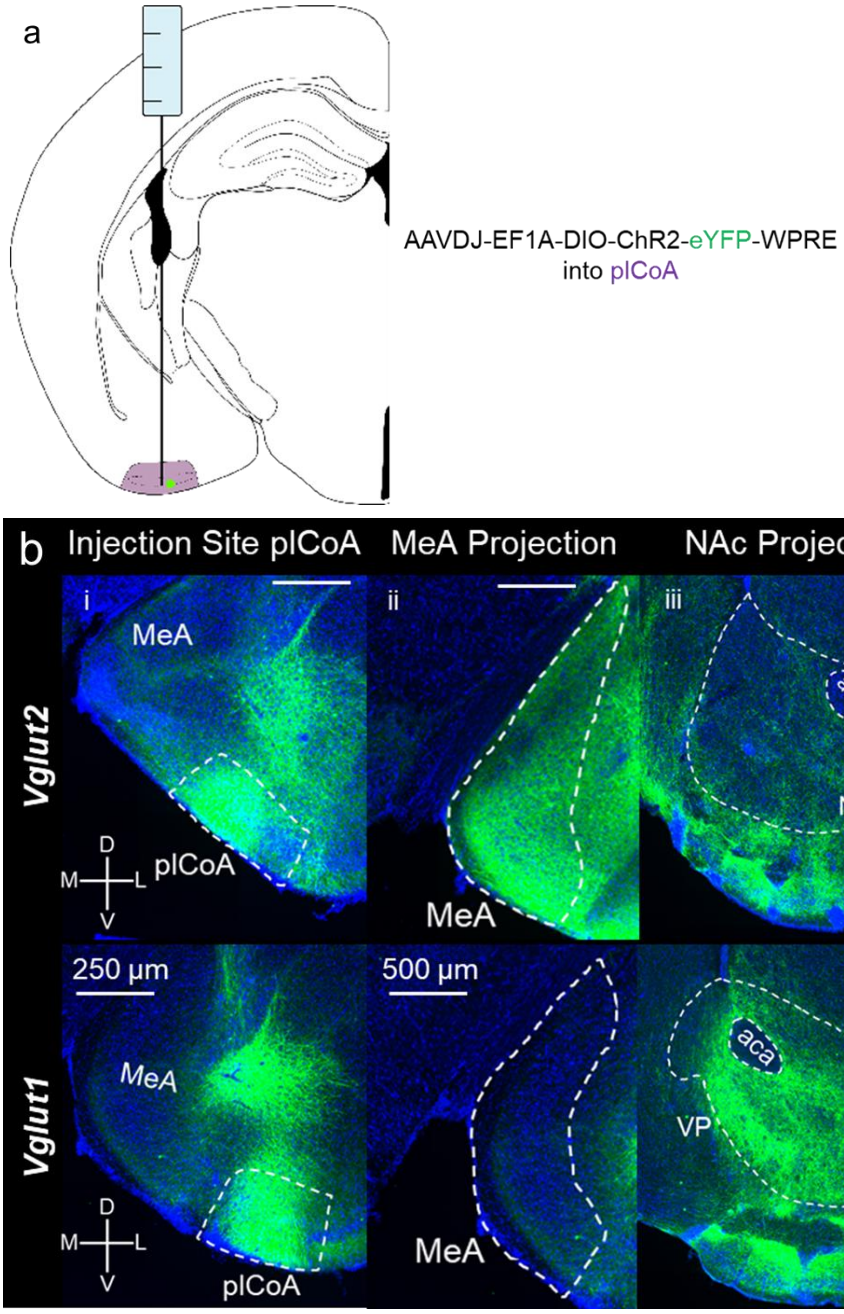
a
AAVDJ-EF1A-DIO-ChR2-eYFP-WPRE
into plCoA
b
Injection Site plCoA
MeA Projection
NAc Projection
i
ii
iii
Vglut2
MeA
plCoA
aca
NAc
OT
D
M
L
V
250 µm
500 µm
500 µm
Vglut1
MeA
plCoA
MeA
VP
NAc
OT
C
Output % from plCoA
30
20
10
0
VGlut2
VGlut1
*
*
**
Pir
MeA
ACo
BNST
OT
PMCo
CxA
AHi
NAc
VP
CeA
EA
AA
LOT
AIV
IPAC
IL

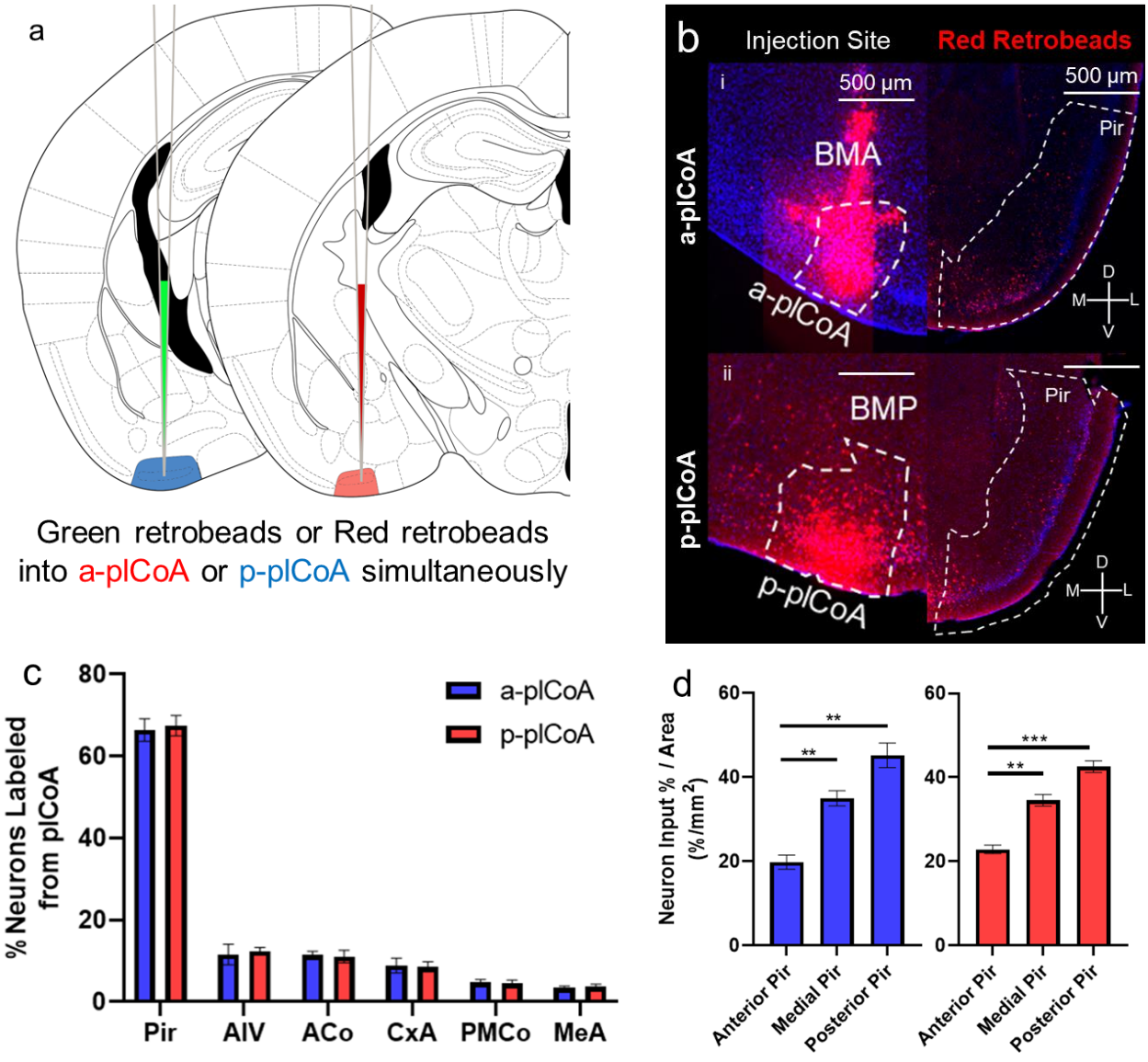

Figure 7 | Retrograde Labeling of a-plCoA and p-plCoA Show Both Structures Receive Input Primarily from the Medial and Posterior Piriform Cortex (Pir). Injection of red and green retrobeads into either the a-plCoA or p-plCoA shows both receive strong input from the medial and posterior Pir. **a**: Schematic of a coronal section showing the injection of green and red retrobeads in either the a-plCoA or p-plCoA in the same animal, suggesting the plCoA does not discriminate on a topographical axis in terms of where it receives its inputs. **b**: Representative images of the red retrobeads (green not shown as it was too difficult to obtain a clear representation) injected in either the a/p-plCoA, along with representative images of the posterior Pir showing inputs received from the a-plCoA (**i**) and p-plCoA (**ii**). **c**: The percentage of neurons labeled from either the a-plCoA or p-plCoA show similar percentages labeled in each structure listed in the bar graph; error bars, s.e.m. **d**: The percentage of neurons per area of the Pir from the a-plCoA or the p-plCoA show both the a-plCoA and p-plCoA receive input primarily from the medial and posterior Pir; $^{**}p < 0.01$, $^{***}p < 0.001$, paired t-test comparing input percentages per Pir area between anterior Pir, medial Pir, and posterior Pir; error bars, s.e.m.

Acknowledgements

The figures section, in full, is currently being prepared for submission for publication of the material. The results and figures section is coauthored by Blanquart, Marlon, Howe VI, James, and Chan, Chung Lung. The thesis author was the primary author of this material.

REFERENCES

Alkaslasi, M. R., Piccus, Z. E., Hareendran, S., Silberberg, H., Chen, L., Zhang, Y., Petros, T. J., & Le Pichon, C. E. (2021). Single nucleus RNA-sequencing defines unexpected diversity of cholinergic neuron types in the adult mouse spinal cord. *Nature Communications*, *12*(1), 2471. https://doi.org/10.1038/s41467-021-22691-2

Allen Institute for Brain Science. (2004). Allen Mouse Brain Atlas. http://mouse.brain-map.org/ Lein, E. S., Hawrylycz, M. J., Ao, N., Ayres, M., Bensinger, A., Bernard, A., Boe, A. F., Boguski, M. S., Brockway, K. S., Byrnes, E. J., Chen, L., Chen, L., Chen, T.-M., Chin, M. C., Chong, J., Crook, B. E., Czaplinska, A., Dang, C. N., Datta, S., Dee, N. R., Desaki, A.I., Desta, T., Diep, E., Dolbeare, T. A., Donelan, M. J., Dong, H. W., Dougherty, J. G., Duncan, B. J., Ebbert, A. J., Eichele, G., Estin, L., Faber C., Facer, B.A., Fields, R., Fischer, S.R., Fliss, T. P., Frensley, C., Gates, S. N., Glattfelder, K. J., Halverson, K. R., Hart, M. R., Hohmann, J. G., Howell, M. P., Jeung, D. P., Johnson, R. A., Karr, P. T., Kawal, R., Kidney, K. D., Lau, C., Lemon, T. A., Liang, A. J., Liu, Y., Lung, L. T., Michaels, J., Morgan, J. J., Morgan, R. J., Mortrud, M. T., Mosqueda, N. F., Ng, L. L., Ng, R., Orta, G. J., Overly, C. C., Pak, T. H., Parry, S. E., Pathak, S. D., Pearson, O. C., Puchalski, R. B., Riley, Z. L., Rockett, H. R., Rowland, S. A., Royall, J. J., Ruiz, M. J., Sarno, N. R., Schaffnit, K., Shapovalova, N. V., Sivisay, T., Slaughterbeck, C. R., Smith, S. C., Smith, K. A., Smith, B. I., Sodt, A. J., Stewart, N. N., Stumpf, K. R., Sunkin, S. M., Sutram, M., Tam, A., Teemer, C. D., Thaller, C., Thompson, C. L., Varnam, L. R., Visel, A., Whitlock, R. M., Wohnoutka, P. E., Wolkey, C. K., Wong, V. Y., Wood, M., Yaylaoglu, M. B., Young, R. C., Youngstrom, B. L., Yuan, X. F., Zhang, B., Zwingman, T. A., Jones, A. R. (2007). Genome-wide atlas of gene expression in the adult mouse brain. *Nature*, *445*(7124), 168–176. https://doi.org/10.1038/nature05453

Arshamian, A., Gerkin, R. C., Kruspe, N., Wnuk, E., Floyd, S., O'Meara, C., Garrido Rodriguez, G., Lundström, J. N., Mainland, J. D., & Majid, A. (2022). The perception of odor pleasantness is shared across cultures. *Current Biology*, *32*(9), 2061-2066.e3. https://doi.org/10.1016/j.cub.2022.02.062

Beyeler, A., Chang, C.-J., Silvestre, M., Lévêque, C., Namburi, P., Wildes, C. P., & Tye, K. M. (2018). Organization of Valence-Encoding and Projection-Defined Neurons in the Basolateral Amygdala. *Cell Reports*, *22*(4), 905–918. https://doi.org/10.1016/j.celrep.2017.12.097

Beyeler, A., Namburi, P., Glober, G. F., Simonnet, C., Calhoon, G. G., Conyers, G. F., Luck, R., Wildes, C. P., & Tye, K. M. (2016). Divergent Routing of Positive and Negative Information from the Amygdala during Memory Retrieval. *Neuron*, *90*(2), 348–361. https://doi.org/10.1016/j.neuron.2016.03.004

Buck, L., & Axel, R. (1991). A novel multigene family may encode odorant receptors: A molecular basis for odor recognition. *Cell*, *65*(1), 175–187. https://doi.org/10.1016/0092-8674(91)90418-x

Buck, L. B. (2004). Olfactory Receptors and Odor Coding in Mammals. *Nutrition Reviews*, *62*, S184–S188. https://doi.org/10.1111/j.1753-4887.2004.tb00097.x

Ghosh, S., Larson, S. D., Hefzi, H., Marnoy, Z., Cutforth, T., Dokka, K., & Baldwin, K. K. (2011). Sensory maps in the olfactory cortex defined by long-range viral tracing of single neurons. *Nature*, *472*(7342), 217–220. https://doi.org/10.1038/nature09945

Haque, A., Engel, J., Teichmann, S. A., & Lönnberg, T. (2017). A practical guide to single-cell RNA-sequencing for biomedical research and clinical applications. *Genome Medicine*, *9*(1), 75. https://doi.org/10.1186/s13073-017-0467-4

Iurilli, G., & Datta, S. R. (2017). Population Coding in an Innately Relevant Olfactory Area. *Neuron*, *93*(5), 1180-1197.e7. https://doi.org/10.1016/j.neuron.2017.02.010

Jensen, E. (2014). Technical Review: In Situ Hybridization: AR Insights. The Anatomical Record, 297(8), 1349–1353. https://doi.org/10.1002/ar.22944

Kandel, E. R. (Ed.). (2013). *Principles of neural science* (5th ed). McGraw-Hill.

Kevetter, G. A., & Winans, S. S. (1981). Connections of the corticomedial amygdala in the golden hamster. II. Efferents of the "olfactory amygdala." *The Journal of Comparative Neurology*, *197*(1), 99–111. https://doi.org/10.1002/cne.901970108

Kim, J., Pignatelli, M., Xu, S., Itohara, S., & Tonegawa, S. (2016). Antagonistic negative and positive neurons of the basolateral amygdala. *Nature Neuroscience*, *19*(12), 1636–1646. https://doi.org/10.1038/nn.4414

Kim, J., Zhang, X., Muralidhar, S., LeBlanc, S. A., & Tonegawa, S. (2017). Basolateral to Central Amygdala Neural Circuits for Appetitive Behaviors. *Neuron*, *93*(6), 1464-1479.e5. https://doi.org/10.1016/j.neuron.2017.02.034

Kobayakawa, K., Kobayakawa, R., Matsumoto, H., Oka, Y., Imai, T., Ikawa, M., Okabe, M., Ikeda, T., Itohara, S., Kikusui, T., Mori, K., & Sakano, H. (2007). Innate versus learned odour processing in the mouse olfactory bulb. *Nature*, *450*(7169), 503–508. https://doi.org/10.1038/nature06281

"Measuring Cell Fluorescence using ImageJ." The Open Lab Book, https://theolb.readthedocs.io/en/latest/imaging/measuring-cell-fluorescence-using-imagej.html. Oct. 2022

Patel, G. H., Kaplan, D. M., & Snyder, L. H. (2014). Topographic organization in the brain: Searching for general principles. *Trends in Cognitive Sciences*, *18*(7), 351–363. https://doi.org/10.1016/j.tics.2014.03.008

Root, C. M., Denny, C. A., Hen, R., & Axel, R. (2014). The participation of cortical amygdala in innate, odour-driven behaviour. *Nature*, *515*(7526), 269–273. https://doi.org/10.1038/nature13897

Stowers, L., & Logan, D. W. (2010). Olfactory mechanisms of stereotyped behavior: On the scent of specialized circuits. *Current Opinion in Neurobiology*, *20*(3), 274–280. https://doi.org/10.1016/j.conb.2010.02.013

Ubeda-Bañon, I., Novejarque, A., Mohedano-Moriano, A., Pro-Sistiaga, P., de la Rosa-Prieto, C., Insausti, R., Martinez-Garcia, F., Lanuza, E., & Martinez-Marcos, A. (2007). Projections from the posterolateral olfactory amygdala to the ventral striatum: Neural basis for reinforcing properties of chemical stimuli. *BMC Neuroscience*, *8*, 103. https://doi.org/10.1186/1471-2202-8-103